Paper: ASAT-16-113-ST

16th International Conference on
AEROSPACE SCIENCES & AVIATION TECHNOLOGY,
ASAT - 16 – May 26 - 28, 2015, E-Mail: asat@mtc.edu.eg
Military Technical College, Kobry Elkobbah, Cairo, Egypt
Tel : +(202) 24025292 – 24036138, Fax: +(202) 22621908

Modeling and Analysis of Laminated Composite Plates Embedded with Shape Memory Alloy Wires

M. Kassem Abbas*, M Adnan Elshafei* , Hany M Negm[+]
* Egyptian Armed Forces
[+] Department of Aerospace Engineering, Cairo University, Cairo, Egypt

Abstract: A Laminated composite plate with embedded shape memory alloy wires are modeled and analyzed based on the modified higher-order shear deformation theory. The Hamilton's principle in conjunction with Brinson's constitutive model is used to obtain the three-dimensional governing equations. The Ritz solution technique is used to get the static response as well as the dynamic characteristics of the proposed plates. A simply-supported and cantilevered plates subjected to mechanical loads are used in the analysis with a prepared program using Mathematica langue. Parametric studies are conducted to demonstrate the effect of plate dimensions, fiber orientation angle and volume fraction of composite fibers and shape memory alloy wires, on the activated plate natural frequencies. The obtained results are compared to the available studies solved by different theories and found convenient.

Keywords: Shape memory alloys, Brinson's model, composite plate, Higher-order shear deformation theory, rule of mixture, Ritz energy method, static and dynamic analysis.

1. Introduction

The Shape memory alloy (SMA) has unique properties of one way shape memory effect (SME), two way shape memory effect, pseudoelasticity and high damping capacity. The SMA wires, strips, or sheets can be surface mounted or embedded in a structure core to form smart composite structure. Intensive researches have been made on SMA wires and bonded sheets working as actuators [1-8]. Ghomshei et al [1-2] proposed a nonlinear finite element model and experimental test for the time response of a shape memory alloy actuator composed of core material with SMA sheets or wires embedded in or bonded to the core part. The model is developed based on a higher order shear deformation theory and the von- Karman strain field equation. A one-dimensional constitutive equation with non-constant material functions and sinusoidal phase transformation kinetics is used to model the thermo-mechanical behavior of the SMA actuator. There are 2 types of martensite depending on the way that causes the transformation: 1st type is temperature induced martensite which caused by decreasing temperature only with free stress and this type doesn't cause recovery stress as shown in Figure A1 number 3, while the 2nd type is stress induced martensite which caused by applying stress and this type generate recovery stress as shown in Figure A1 number 1-a and 1-b. Balapgol et al [3-4] studied the deflection, natural frequency and time response of a laminated composite plate consists of thin layer of SMA bonded to elastomer core using finite element method based on the first order shear deformation theory.

They concluded that the input power heat sink strength, thermal conductivity, and thickness of the elastomer layer play important roles for controlling the time response of the SMA laminated actuator. Gordaninejad et al [5] presented a two- dimensional finite element model based on classical lamination theory, energy equations, and two- dimensional transition model of SMA layer for the response
of thermally driven SMA / elastomer actuator. Wu et al [6]derived closed form solutions for the stress-strain-temperature response of thermally driven shape memory alloy composite actuator neglecting the heat conduction in axial direction. Rogers et al [7] used the Rayleigh-Ritz method to perform a linear analysis for simply-supported plate embedded with SMA fibers. They studied the plate deflection, free vibration, buckling, and acoustic control. Lin et al [8] proposed a closed form solution for symmetric composite beams embedded with SMA fibers with various boundary conditions. The resultant actuation forces and normal stress distribution were calculated for the proposed beams. Several constitutive models have been proposed to predict the thermo-mechanical response of the SMA. One of the earliest models is the one-dimensional Tanaka's model [9], which is macroscopic model that is derived from thermodynamic concepts and through experimental observations. This means that the transformation doesn't take action suddenly at one type, it takes time to gradually transform from full austenite phase $\xi = 0$ to full martensite phase $\xi = 1$. The evolutionary equation is expressed using exponential function in the form of $\xi = \xi(\sigma, T)$. Tanaka's model is expressed its ability to characterize most of the behaviors of the SMA. Liang and Rogers [10] improved Tanaka's model by directly matching experimental results to get the evolutionary equation which is expressed using the cosine function. The constitutive equation of their model remains the same while parameters of the equations are determined through experiments. A major improvement of the Tanaka's model was made by Brinson [11-12], who's recognized that not all martensite that are converted to austenite will produce the recovery stress, but only the stress induced martensite (SIM) that is responsible for the shape memory effect. Consequently, the martensite fraction is divided into two parts: stress induced martensite and temperature induced martensite. This model also did not assume constant material functions in the constitutive relationship. Furthermore, Brinson's model made some amendment that the constitutive equation will be valid at any temperature, and gave a better representation of the SMA behaviors compared to the Liang and Rogers's model, and it is quite popular for engineering applications because it is simple, accurate and easy to implement into numerical applications. In the present work, a mathematical formulation for composite plate with embedded SMA wires is deduced using the higher order shear deformation theory and SMA Brinson's constitutive model. Hamilton's principle is used to obtain the governing equations of motion. The effect on the SMA material constants, thermal stresses, and the recovery stress is considered for the proposed composite plate. The SMA wire layer is treated as an orthotropic layer similar to typical graphite/epoxy layers. The effective properties are determined using the rule of mixture, except that both the material properties and the recovery stress of the SMA wires are functions of the martensite phase fraction ξ. The SMA recovery stress values are expressed in the governing equation as external force[13], and computed using Brinson's model as a function of the temperature applied to the SMA composite plates. Parametric studies are conducted to demonstrate the effect of plate dimensions, fiber orientation angle and volume fraction of composite fibers and shape memory alloy wires on the activated plate natural frequencies. The obtained results are compared to the available studies solved by different theories and found convenient.

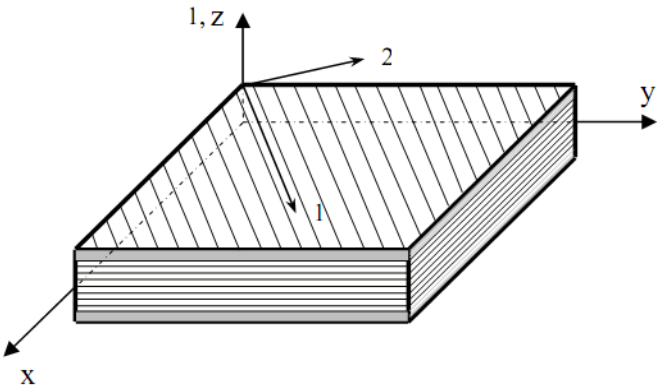

Figure 1. SMA composite plates layers
(:Nitinol-epoxy, : graphite/epoxy)

2. SMA Brinson's constitutive model

The Brinson's constitutive model assumes that the phase transformation depends only on temperature and stress [11] and volume fraction of martensite, ξ_S. A two equations namely the constitutive equation and the evolutionary equations are used to solve Brinson's model. Brinson divides the martensitic volume fraction into two parts:

$$\xi = \xi_S + \xi_T \tag{1}$$

where ξ_S corresponds to the fraction of the stress induced martensite (SIM) and ξ_T refers to the fraction of the temperature induced martensite (TIM), Thus:

$$\sigma = \sigma(\varepsilon, \xi_S, \xi_T, T) \tag{2}$$

Making simple derivation and applying force condition, Brinson's model for constant material parameter can be expressed as [12]:

$$\sigma - \sigma_0 = D(\varepsilon - \varepsilon_0) + \Omega(\xi_S - \xi_{S0}) + \theta(T - T_0) \tag{3}$$

where D is the Young Modulus, θ is the thermo-elastic tensor and Ω is the transformation tensor. The effect of the stress on the transition temperature must consider the conversion of TIM to SIM. This process of conversion starts when TIM is exposed to stress σ_s^{cr}, and ends at a stress value of σ_f^{cr}. The values of these critical stresses can be determined either by experiment, or theoretical using a model based on the potential energy necessary to overcome the chemical energy barrier for conversion of twins as done by Achenbach and Muller [14]. The stress temperature coefficients C_A and C_M in Brinson's model are not assumed to be equal and both are determined by experiment. The effect of stress on the critical temperature is shown in Figure A1. Thus the evolution equations that represent ξ_S and ξ_T as functions of stress and temperature Eq. (4) and given in the Appendix A [12]:

$$\xi_S = \sigma(\varepsilon, \xi_S, \xi_T, T) \tag{4}$$

3. Displacement Field

The displacement field equations of the modified higher order shear deformation theory (MHSDT) are represented by:

$$u(x,y,z,t)=u_0(x,y,t)+z\left(\theta_x(x,y,t)-\frac{\partial w_0(x,y,t)}{\partial x}\right)+z^2\psi_x(x,y,t)+z^3\xi_x(x,y,t)$$
$$v(x,y,z,t)=v_0(x,y,t)+z\left(\theta_y(x,y,t)-\frac{\partial w_0(x,y,t)}{\partial y}\right)+z^2\psi_y(x,y,t)+z^3\xi_y(x,y,t)$$
$$w(x,y,z,t)=w_0(x,y,t)+z\,\theta_z(x,y,t)+z^2\psi_z(x,y,t) \tag{5}$$

The displacement field Eq.(5) can be written in matrix form as follows:

$$\{U\}=\{U^0\}+z\{U^1\}+z^2\{U^2\}+z^3\{U^3\} \tag{6}$$

where

$$\{U^0\}^T=[u_0 \quad v_0 \quad w_0],\{U^1\}^T=\left[\theta_x-\frac{\partial w_0}{\partial x} \quad \theta_y-\frac{\partial w_0}{\partial y} \quad \theta_z\right],$$
$$\{U^2\}^T=[\psi_x \quad \psi_y \quad \psi_z],\{U^3\}^T=[\xi_x \quad \xi_y \quad 0] \tag{7}$$

4. Strain-Displacement Relationships

The strain-displacement relationships can be expressed in a matrix form as follows:

$$\{\varepsilon\}=\{\varepsilon^0\}+z\{\varepsilon^1\}+z^2\{\varepsilon^2\}+z^3\{\varepsilon^3\} \tag{8}$$

where

$$\{\varepsilon\}^T=[\varepsilon_{xx} \quad \varepsilon_{yy} \quad \varepsilon_{zz} \quad \gamma_{yz} \quad \gamma_{zx} \quad \gamma_{xy}] \tag{9}$$

$$\{\varepsilon^0\}^T=\left[\frac{\partial u_0}{\partial x} \quad \frac{\partial v_0}{\partial y} \quad \theta_z \quad \theta_y \quad \theta_x \quad \frac{\partial u_0}{\partial y}+\frac{\partial v_0}{\partial x}\right]$$
$$\{\varepsilon^1\}^T=\left[\frac{\partial\theta_x}{\partial x}-\frac{\partial^2 w_0}{\partial x^2} \quad \frac{\partial\theta_y}{\partial y}-\frac{\partial^2 w_0}{\partial y^2} \quad 2\psi_z \quad 2\psi_y+\frac{\partial\theta_z}{\partial y} \quad 2\psi_x+\frac{\partial\theta_z}{\partial x} \quad \frac{\partial\theta_x}{\partial y}+\frac{\partial\theta_y}{\partial x}-2\frac{\partial^2 w_0}{\partial x\,\partial y}\right]$$
$$\{\varepsilon^2\}^T=\left[\frac{\partial\psi_x}{\partial x} \quad \frac{\partial\psi_y}{\partial y} \quad 0 \quad 3\xi_y+\frac{\partial\psi_z}{\partial y} \quad 3\xi_x+\frac{\partial\psi_z}{\partial x} \quad \frac{\partial\psi_x}{\partial y}+\frac{\partial\psi_y}{\partial x}\right]$$
$$\{\varepsilon^3\}^T=\left[\frac{\partial\xi_x}{\partial x} \quad \frac{\partial\xi_y}{\partial y} \quad 0 \quad 0 \quad 0 \quad \frac{\partial\xi_x}{\partial y}+\frac{\partial\xi_y}{\partial x}\right] \tag{10}$$

5. Stress-strain Relationship

The constitutive relationship for an embedded SMA layer is:

$$\{\sigma_1\}=[Q](\{\varepsilon_1\}-\{\alpha_1\}\Delta T)+V_s\{\sigma_1^r\} \tag{11}$$

where $\{\sigma_1\}$, $\{\varepsilon_1\}$, $[Q]$, $\{\alpha_1\}$, and $\{\sigma_1^r\}$ are the stress vector, strain vector, lamina stiffness matrix, thermal expansion coefficients vector, and SMA recovery stress vector, respectively with respect to principle material axes before transformation. The stiffness matrix of the SMA lamina is calculated using the SMA effective properties determined by the rule of

mixture [15-16] which are function of martensite fraction of SMA ξ. The vectors $\{\alpha_1\}$ and $\{\sigma_1^r\}$ are defined as follows:

$$\{\alpha_1\}^T = [\alpha_1 \quad \alpha_2 \quad \alpha_3 \quad 0 \quad 0 \quad 0] \tag{12}$$

$$\{\sigma_1^r\}^T = [\sigma_r \quad 0 \quad 0 \quad 0 \quad 0 \quad 0] \tag{13}$$

The transformed stress-strain relations for an orthotropic lamina oriented are given by:

$$\begin{Bmatrix} \sigma_x \\ \sigma_y \\ \sigma_z \\ \tau_{yz} \\ \tau_{zx} \\ \tau_{xy} \end{Bmatrix} = \begin{bmatrix} \bar{Q}_{11} & \bar{Q}_{12} & \bar{Q}_{13} & 0 & 0 & \bar{Q}_{16} \\ \bar{Q}_{21} & \bar{Q}_{22} & \bar{Q}_{23} & 0 & 0 & \bar{Q}_{26} \\ \bar{Q}_{31} & \bar{Q}_{32} & \bar{Q}_{33} & 0 & 0 & \bar{Q}_{36} \\ 0 & 0 & 0 & \bar{Q}_{44} & \bar{Q}_{45} & 0 \\ 0 & 0 & 0 & \bar{Q}_{54} & \bar{Q}_{55} & 0 \\ \bar{Q}_{61} & \bar{Q}_{62} & \bar{Q}_{63} & 0 & 0 & \bar{Q}_{66} \end{bmatrix} \left(\begin{Bmatrix} \varepsilon_x \\ \varepsilon_y \\ \varepsilon_z \\ \gamma_{yz} \\ \gamma_{zx} \\ \gamma_{xy} \end{Bmatrix} - \begin{Bmatrix} \alpha_x \\ \alpha_y \\ \alpha_z \\ 0 \\ 0 \\ \alpha_{xy} \end{Bmatrix} \Delta T \right) + V_s \begin{Bmatrix} \sigma_x^r \\ \sigma_y^r \\ 0 \\ 0 \\ 0 \\ \sigma_{xy}^r \end{Bmatrix} \tag{14}$$

where $\bar{Q}_{ij}$ are the transformed stiffness coefficients of the [15-17], $\{\alpha_i\}$ and $\{\sigma_i^r\}$ are the vectors of thermal expansion coefficients and SMA recovery stress, respectively given in Appendix B [15].

6. Energy Formulation

The governing equation of the smart plate is derived using Hamilton's principle [15]:

$$0 = \int_0^T (\delta U + \delta V - \delta K) dt \tag{15}$$

where δU is the virtual strain energy, δV is the virtual work done by the applied forces, and δK is the virtual kinetic energy of the whole structure system.

The virtual strain energy δU of the plate with cross section area A and thickness h is given by [15]:

$$\delta U = \int_A \left\{ \int_{-\frac{h}{2}}^{\frac{h}{2}} \delta\{\varepsilon\}^T \{\sigma\} dz \right\} dxdy \tag{16}$$

By substituting Eq.(14) in Eq.(16) for a number of layers k :

$$\delta U = \int_A \left\{ \sum_{i=1}^{k} \int_{z_{i-1}}^{z_i} \delta\{\varepsilon\}^T \left[[\bar{Q}]_i \left(\{\varepsilon\} - \{\alpha\}_i \Delta T \right) + V_s \{\sigma^r\}_i \right] dz \right\} dxdy \tag{17}$$

where $[\bar{Q}]_i$, $\{\alpha\}_i$, $\{\sigma^r\}_i$ are the stiffness matrix, thermal expansion coefficients and SMA recovery stress vectors. z_i, z_{i+1} are the lower and upper z-coordinates of layer number i measured from mid-plane, respectively. The terms in Eq.(17) are defined as:

$$\delta U = \delta U_m - \delta U_T + \delta U_r \tag{18}$$

Where $\delta U_m - \delta U_T + \delta U_r$ are the mechanical, thermal, and recovery stress components of the strain energy given as follows:

$$\delta U_m = \int_A \left\{ \sum_{i=1}^{k} \int_{z_{i-1}}^{z_i} \delta\{\varepsilon\}^T \left[\bar{Q}\right]_i \{\varepsilon\} dz \right\} dxdy$$

$$\delta U_T = \int_A \left\{ \sum_{i=1}^{k} \int_{z_{i-1}}^{z_i} \delta\{\varepsilon\}^T \left[\bar{Q}\right]_i \{\alpha\}_i \Delta T dz \right\} dxdy \tag{19}$$

$$\delta U_r = \int_A \left\{ \sum_{i=1}^{k} \int_{z_{i-1}}^{z_i} \delta\{\varepsilon\}^T V_s \{\sigma^r\}_i dz \right\} dxdy$$

Substituting Eq.(8) into Eq.(18) yields the virtual strain energy due to mechanical applied load is given as:

$$\delta U_m = \int_A \left\{ \begin{array}{l} \sum_{i=1}^{k} \int_{z_{i-1}}^{z_i} \left(\delta\{\varepsilon^0\}^T + z\,\delta\{\varepsilon^1\}^T + z^2 \delta\{\varepsilon^2\}^T + z^3 \delta\{\varepsilon^3\}^T \right) \left[\bar{Q}\right]_i \\ \left(\{\varepsilon^0\} + z\,\{\varepsilon^1\} + z^2 \{\varepsilon^2\} + z^3 \{\varepsilon^3\} \right) dz \end{array} \right\} dxdy \tag{20}$$

The virtual strain energy due to the thermal load is expressed as:

$$\delta U_T = \int_A \left\{ \sum_{i=1}^{k} \int_{z_{i-1}}^{z_i} \left(\delta\{\varepsilon^0\}^T + z\,\delta\{\varepsilon^1\}^T + z^2 \delta\{\varepsilon^2\}^T + z^3 \delta\{\varepsilon^3\}^T \right) \left[\bar{Q}\right]_i \{\alpha\}_i \Delta T dz \right\} dxdy \tag{21}$$

The virtual strain energy due to the recovery stress is represented by:

$$\delta U_r = \int_A \left\{ \sum_{i=1}^{k} \int_{z_{i-1}}^{z_i} \left(\delta\{\varepsilon^0\}^T + z\,\delta\{\varepsilon^1\}^T + z^2 \delta\{\varepsilon^2\}^T + z^3 \delta\{\varepsilon^3\}^T \right) V_s \{\sigma^r\}_i dz \right\} dxdy \tag{22}$$

Eq.(20) can be rewritten as:

$$\delta U_m = \int_A \left\{ \begin{array}{l} \delta\{\varepsilon^0\}^T [A]\{\varepsilon^0\} + \delta\{\varepsilon^0\}^T [B]\{\varepsilon^1\} + \delta\{\varepsilon^0\}^T [D]\{\varepsilon^2\} \\ + \delta\{\varepsilon^0\}^T [E]\{\varepsilon^3\} + \delta\{\varepsilon^1\}^T [B]\{\varepsilon^0\} + \delta\{\varepsilon^1\}^T [D]\{\varepsilon^1\} \\ + \delta\{\varepsilon^1\}^T [E]\{\varepsilon^2\} + \delta\{\varepsilon^1\}^T [F]\{\varepsilon^3\} + \delta\{\varepsilon^2\}^T [D]\{\varepsilon^0\} \\ + \delta\{\varepsilon^2\}^T [E]\{\varepsilon^1\} + \delta\{\varepsilon^2\}^T [F]\{\varepsilon^2\} + \delta\{\varepsilon^2\}^T [H]\{\varepsilon^3\} \\ + \delta\{\varepsilon^3\}^T [E]\{\varepsilon^0\} + \delta\{\varepsilon^3\}^T [F]\{\varepsilon^1\} + \delta\{\varepsilon^3\}^T [H]\{\varepsilon^2\} \\ + \delta\{\varepsilon^3\}^T [J]\{\varepsilon^3\} \end{array} \right\} dxdy \tag{23}$$

where

$$\left([A],[B],[D],[E],[F],[H],[J]\right) = \sum_{i=1}^{k} \int_{z_{i-1}}^{z_i} \left[\bar{Q}\right]_i \left(1, z, z^2, z^3, z^4, z^5, z^6\right) dz \tag{24}$$

And equation (21) can be rewritten as:

$$\delta U_T = \int_A \left\{ \delta\{\varepsilon^0\}^T \left[A^\alpha\right] + \delta\{\varepsilon^1\}^T \left[B^\alpha\right] + \delta\{\varepsilon^2\}^T \left[D^\alpha\right] + \delta\{\varepsilon^3\}^T \left[E^\alpha\right] \right\} dxdy \tag{25}$$

where

$$\left(\left[A^\alpha\right],\left[B^\alpha\right],\left[D^\alpha\right],\left[E^\alpha\right]\right) = \sum_{i=1}^{k} \int_{z_{i-1}}^{z_i} \left[\bar{Q}\right]_i \{\alpha\}_i \Delta T \left(1, z, z^2, z^3\right) dz \tag{26}$$

Also equation (22) can be rewritten as:

$$\delta U_r = \int_A \left\{ \delta\left\{\varepsilon^0\right\}^T \left[A^r\right] + \delta\left\{\varepsilon^1\right\}^T \left[B^r\right] + \delta\left\{\varepsilon^2\right\}^T \left[D^r\right] + \delta\left\{\varepsilon^3\right\}^T \left[E^r\right] \right\} dxdy \tag{27}$$

where

$$\left(\left[A^r\right],\left[B^r\right],\left[D^r\right],\left[E^r\right]\right) = \sum_{i=1}^{k} \int_{z_{i-1}}^{z_i} V_s \left\{\sigma^r\right\}_i \left(1, z, z^2, z^3\right) dz \tag{28}$$

The virtual work δV done by the applied mechanical loads is given by[18]:

$$\delta V = \int_A \left\{ p_z\left(x,y\right) \delta w\left(x,y,t\right) \right\} dxdy + F_{zi} \delta w\left(x_i, y_i, t\right) \tag{29}$$

where $p_z\left(x,y\right)$ is the transverse distributed load and F_{z_i} is the transverse concentrated force at point i . The virtual kinetic energy δK can be written as [15]:

$$\delta K = \int_V \rho \left[\delta\left\{\dot{U}\right\}^T \left\{\dot{U}\right\} \right] dV \tag{30}$$

where

$$\left\{U\right\}^T = \left[u \quad v \quad w\right] \tag{31}$$

For k layers Eq.(30) is represented as:

$$\delta K = \int_A \left\{ \sum_{i=1}^{k} \int_{z_{i-1}}^{z_i} \rho_i \left[\delta\left\{\dot{U}\right\}^T \left\{\dot{U}\right\} \right] dz \right\} dxdy \tag{32}$$

where ρ_i is the density of layer number i .

Substituting Eq.(6) into Eq.(32), one can obtain;

$$\delta K = \int_A \begin{pmatrix} I_0 \delta\left\{\dot{U}^0\right\}^T \left\{\dot{U}^0\right\} + I_1 \delta\left\{\dot{U}^0\right\}^T \left\{\dot{U}^1\right\} + I_2 \delta\left\{\dot{U}^0\right\}^T \left\{\dot{U}^2\right\} + I_3 \delta\left\{\dot{U}^0\right\}^T \left\{\dot{U}^3\right\} \\ + I_1 \delta\left\{\dot{U}^1\right\}^T \left\{\dot{U}^0\right\} + I_2 \delta\left\{\dot{U}^1\right\}^T \left\{\dot{U}^1\right\} + I_3 \delta\left\{\dot{U}^1\right\}^T \left\{\dot{U}^2\right\} + I_4 \delta\left\{\dot{U}^1\right\}^T \left\{\dot{U}^3\right\} \\ + I_2 \delta\left\{\dot{U}^2\right\}^T \left\{\dot{U}^0\right\} + I_3 \delta\left\{\dot{U}^2\right\}^T \left\{\dot{U}^1\right\} + I_4 \delta\left\{\dot{U}^2\right\}^T \left\{\dot{U}^2\right\} + I_5 \delta\left\{\dot{U}^2\right\}^T \left\{\dot{U}^3\right\} \\ + I_3 \delta\left\{\dot{U}^3\right\}^T \left\{\dot{U}^0\right\} + I_4 \delta\left\{\dot{U}^3\right\}^T \left\{\dot{U}^1\right\} + I_5 \delta\left\{\dot{U}^3\right\}^T \left\{\dot{U}^2\right\} + I_6 \delta\left\{\dot{U}^3\right\}^T \left\{\dot{U}^3\right\} \end{pmatrix} dxdy \tag{33}$$

where

$$\left(I_0, I_1, I_2, I_3, I_4, I_5, I_6\right) = \sum_{i=1}^{k} \int_{z_{i-1}}^{z_i} \rho_i \left(1, z, z^2, z^3, z^4, z^5, z^6\right) dz \tag{34}$$

7. Ritz Solution Technique

The unknown displacements $u_0, v_0, w_0, \theta_x, \theta_y, \theta_z, \psi_x, \psi_y, \psi_z\ \xi_x, \xi_y$ of the given problem are approximated by (x-y) dependent functions that satisfy the geometric boundary conditions as follows:

$$\gamma_i\left(x,y,t\right) = \left\{a_i\left(x,y\right)\right\}^T \left\{q_i\left(t\right)\right\} \qquad i = 1, 2 \ldots 11 \tag{35}$$

where $\gamma_i(x,y,t)$ represents the unknown displacements $u_0, v_0, w_0, \theta_x, \theta_y, \theta_z, \psi_x, \psi_y, \psi_z$ ξ_x, ξ_y, while $\{a_i(x,y)\}$ are column vectors of the Ritz approximation functions that satisfy the boundary conditions of the plate and $\{q_i(t)\}$ are the column vector of the Ritz coefficients to be determined. The present study presents both simply supported and cantilevered boundary conditions. The used Ritz functions $\{a_i(x,y)\}$ are listed in Appendices C and D, respectively.

8. Equations of Motion

The equations of motion are derived using the Ritz approximation technique for the eleven DOF. based on the displacement field equations. By inserting $\{\varepsilon^0\}$, $\{\varepsilon^1\}$, $\{\varepsilon^2\}$, and $\{\varepsilon^3\}$ in terms of the generalized coordinates $\{q_i\}$ in equations (23), (25), and (27) yields to:

$$\delta U_m = \delta\{q(t)\}^T [K]\{q(t)\} \tag{36}$$

where $[K]$ is the laminate stiffness matrix.

$$[K] = \int_A \begin{Bmatrix} [\bar{\varepsilon}^0]^T [A][\bar{\varepsilon}^0] + [\bar{\varepsilon}^0]^T [B][\bar{\varepsilon}^1] + [\bar{\varepsilon}^0]^T [D][\bar{\varepsilon}^2] + [\bar{\varepsilon}^0]^T [E][\bar{\varepsilon}^3] \\ + [\bar{\varepsilon}^1]^T [B][\bar{\varepsilon}^0] + [\bar{\varepsilon}^1]^T [D][\bar{\varepsilon}^1] + [\bar{\varepsilon}^1]^T [E][\bar{\varepsilon}^2] + [\bar{\varepsilon}^1]^T [F][\bar{\varepsilon}^3] \\ + [\bar{\varepsilon}^2]^T [D][\bar{\varepsilon}^0] + [\bar{\varepsilon}^2]^T [E][\bar{\varepsilon}^1] + [\bar{\varepsilon}^2]^T [F][\bar{\varepsilon}^2] + [\bar{\varepsilon}^2]^T [H][\bar{\varepsilon}^3] \\ + [\bar{\varepsilon}^3]^T [E][\bar{\varepsilon}^0] + [\bar{\varepsilon}^3]^T [F][\bar{\varepsilon}^1] + [\bar{\varepsilon}^3]^T [H][\bar{\varepsilon}^2] + [\bar{\varepsilon}^3]^T [J][\bar{\varepsilon}^3] \end{Bmatrix} dxdy \tag{37}$$

Equation (25)will be:

$$\delta U_T = \delta\{q(t)\}^T \{F_T\} \tag{38}$$

where $\{F_T\}$ is the thermal load vector.

$$\{F_T\}^T = \int_A \left\{ [\bar{\varepsilon}^0]^T [A^\alpha] + [\bar{\varepsilon}^1]^T [B^\alpha] + [\bar{\varepsilon}^2]^T [D^\alpha] + [\bar{\varepsilon}^3]^T [E^\alpha] \right\} dxdy \tag{39}$$

Equation (27) will be:

$$\delta U_r = \delta\{q(t)\}^T \{F_r\} \tag{40}$$

where $\{F_r\}$ is the recovery stress load vector.

$$\{F_r\}^T = \int_A \left\{ [\bar{\varepsilon}^0]^T [A^r] + [\bar{\varepsilon}^1]^T [B^r] + [\bar{\varepsilon}^2]^T [D^r] + [\bar{\varepsilon}^3]^T [E^r] \right\} dxdy \tag{41}$$

The virtual work δV done by the applied forces can be written as:

$$\delta V = \delta\{q\}^T \left(\{F\} + \{F_0\}\right) \tag{42}$$

where $\{F\}$ and $\{F_0\}$ is the distributed and concentrated load vectors, respectively given by,

$$\{F\}^T = \int_A \begin{bmatrix} 0 & 0 & p_z(x,y)\{a_3\}^T & 0 & 0 & 0 & 0 & 0 & 0 & 0 & 0 \end{bmatrix} dxdy$$
$$\{F_0\}^T = \begin{bmatrix} 0 & 0 & F_{zi}\{a_3(x_i,y_i)\}^T & 0 & 0 & 0 & 0 & 0 & 0 & 0 & 0 \end{bmatrix} \quad (43)$$

The virtual kinetic energy δW is expressed as follows:

$$\delta W = \delta\{\dot{q}(t)\}^T [M]\{\dot{q}(t)\} \quad (44)$$

where $[M]$ is the mass matrix of the laminate

$$[M] = \int_A \begin{pmatrix} I_0[\bar{U}^0]^T[\bar{U}^0] + I_1[\bar{U}^0]^T[\bar{U}^1] + I_2[\bar{U}^0]^T[\bar{U}^2] + I_3[\bar{U}^0]^T[\bar{U}^3] \\ +I_1[\bar{U}^1]^T[\bar{U}^0] + I_2[\bar{U}^1]^T[\bar{U}^1] + I_3[\bar{U}^1]^T[\bar{U}^2] + I_4[\bar{U}^1]^T[\bar{U}^3] \\ +I_2[\bar{U}^2]^T[\bar{U}^0] + I_3[\bar{U}^2]^T[\bar{U}^1] + I_4[\bar{U}^2]^T[\bar{U}^2] + I_5[\bar{U}^2]^T[\bar{U}^3] \\ +I_3[\bar{U}^3]^T[\bar{U}^0] + I_4[\bar{U}^3]^T[\bar{U}^1] + I_5[\bar{U}^3]^T[\bar{U}^2] + I_6[\bar{U}^3]^T[\bar{U}^3] \end{pmatrix} dxdy \quad (45)$$

By substituting equations (18), (36), (38), (40), (42), and (44) in Eq.(15) the whole structure equation of motion is represented by:

$$[M]\{\ddot{q}\} + [K]\{q\} = \{F\} + \{F_0\} + \{F_T\} + \{F_r\} \quad (46)$$

$[K]$ is the stiffness matrix, $[M]$ is the mass matrix, $\{F\}$ and $\{F_0\}$ are the distributed and concentrated load vectors, $\{F_T\}$ and $\{F_r\}$ are the thermal and recovery stress load vectors, respectively. The unknown $\{q\}$ is the Ritz coefficients to be determined.

9. Numerical examples and Discussion

The static and dynamic responses of the proposed plate are presented [19-20]. Parametric studies are conducted to investigate the effect of plate's dimensions, orientation and volume fraction of composite fibers and shape memory alloy wires on the activated plate natural frequencies. A simply supported and cantilever plates are used in these studies. A set of computer programs developed by Mathematica 7 is used in this study.

A multi-layered composite plate with embedded SMA wires is illustrated in Figure 2. The plate under consideration is made of 12 unidirectional composite material layers (i.e. 2 SMA/epoxy and 10 graphite/epoxy layers). The length and the width of the plate are both 500 mm, whereas the thickness h is 9 mm. The thickness of each SMA/epoxy layer is 0.5 mm, whereas the thickness of each graphite/ epoxy layer is 0.8 mm. The orientation angle of the SMA wires within the SMA/epoxy layers, and the graphite fibers within the graphite/epoxy layers of the plate are defined by the angles α and β, respectively. It is also assumed that the SMA/epoxy layers are symmetrically placed as two outer layers with the plate mid-plane as shown in Figure 2. The relative volume fraction of the SMA wires and the graphite fibers within each layer of the plate is 0.5. The ply stacking sequence of the plate is $[0°/(\pm 45°)_5/0°]$. The mechanical properties of the SMA wires and the graphite/epoxy composite are given in Table 1. A two different types of plate boundary conditions are investigated: cantilever plate (i.e. one edge of the plate clamped along the y-axis), and simply-supported plate (along its four edges). The obtained results are presented as relative values (i.e. the relative fundamental natural frequency). They are defined as ratios of the fundamental natural frequency calculated when the SMA wires are activated to the values when they are not activated.

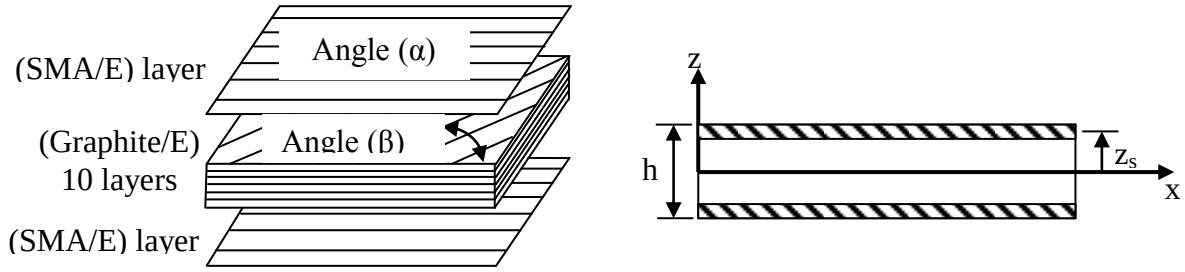

Figure 2. The geometry of the multilayered composite plate with SMA wires.

Table 1. Mechanical properties of composite material and SMA wires [21].

Material	Young's modulus [GPa]	Poisson's ratio	Density [kg/m^3]
Epoxy resin	3.43	0.35	1250.0
Graphite fibers	275.6	0.20	1900.0
SMA–martensite	26.3	0.30	6448.1
SMA–austenite	67.0	0.30	

The changes in the relative fundamental natural frequency of the plate are presented in Figure 3 and Figure 4, as a function of the plate dimensions. It is assumed that the plate length a, and the width b, of the plate can vary in this case, whereas the thickness of the plate h remains unchanged (changes in the dimensions of the plate obviously also result in changes in the plate mass). It can be seen that both the dimensions of the plate as well as the boundary condition type, have a great influence on the relative fundamental natural frequency of the plate. For the cantilever plate, the relative fundamental natural frequency of the plate increases due to the activation of the SMA wires towards a longer and narrower plate. The maximum relative fundamental natural frequency of the plate is, in this case, obtained for a beam-like structure, for which the SMA wires within the SMA/epoxy layers are lengthwise orientated. Contrary to this, the relative fundamental natural frequency of the simply-supported plate, increases towards a wider and shorter plate. The maximum relative fundamental natural frequency is obtained for a beam-like structure for which the SMA wires within the SMA/epoxy layers are widthwise orientated. It is clear from, Figure 3 and Figure 4 that the obtained results are very comparable with the published data obtained by Zak using the finite element technique with a mish size 8X8, [21]. It should be emphasized that the maximum changes in the relative fundamental natural frequency of the plate are observed in the case when the minimum number of constraints is imposed by the chosen boundary condition. Consequently, the maximum changes in the relative fundamental natural frequency are observed for the cantilever plate.

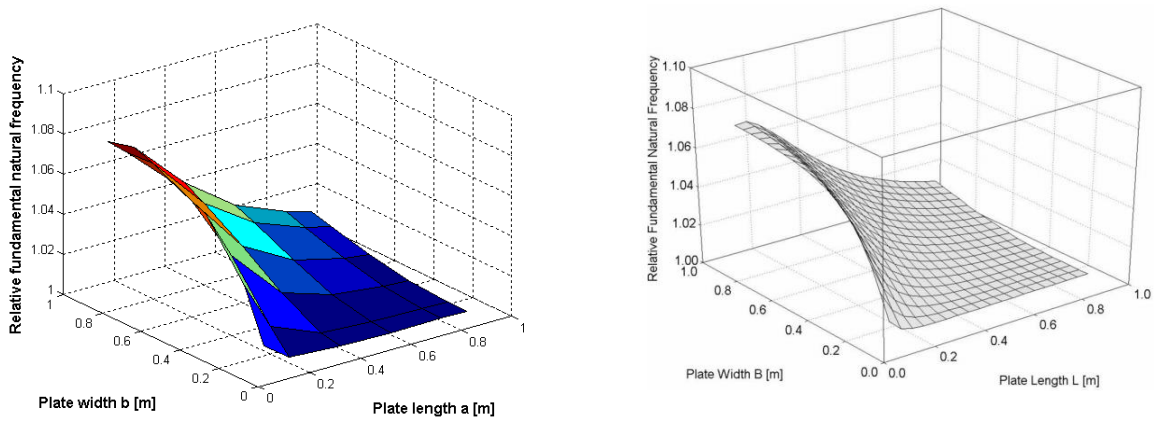

(a) Present model **(b) Zak [21]**

Figure 3. Change in the relative fundamental frequency of a simply-supported plate as a function of its dimensions.

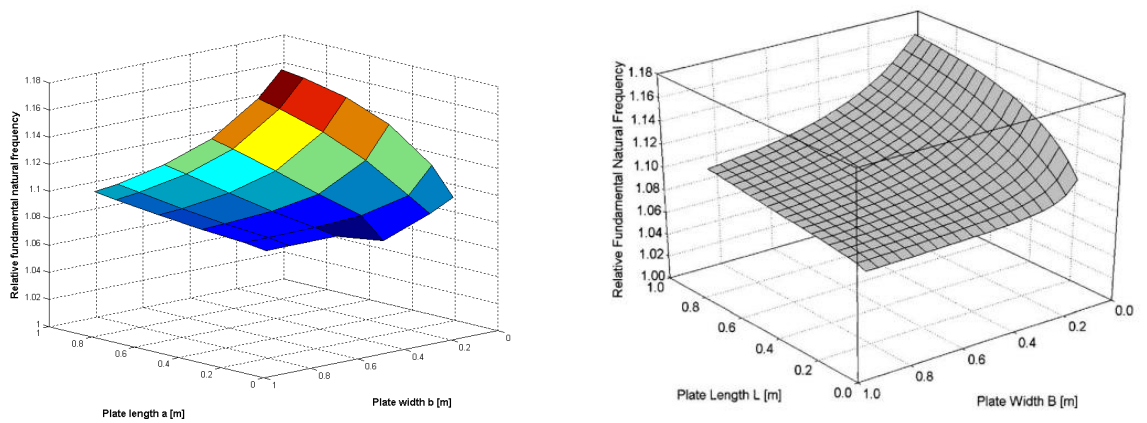

(a) Present model **(b) Zak [21]**

Figure 4. Change in the relative fundamental natural frequency of a cantilever plate as a function of its dimensions

In Figure 5 and Figure 6 results for changes in the relative fundamental natural frequency of the plate are presented as a function of the orientation angle of the SMA wires within the SMA/epoxy layers, as well as the orientation angle of the graphite fibers within the graphite/ epoxy layers of the plate. The ply stacking sequence of the plate considered here can be defined as $[\alpha/(\beta/(\beta\text{-}90°)_5/\ \alpha]$, where α denotes the orientation angle of the SMA wires within the SMA/epoxy layers, while β denotes the orientation angle of the graphite fibers within the graphite/epoxy layers. It is assumed that all other mechanical properties of the plate remain unchanged in this case. It is seen from Figure 5 and Figure 6 that the relative fundamental natural frequency of the cantilever plate decreases rapidly with an increase in the orientation angle of the SMA wires within the SMA/epoxy layers of the plate from 0° to 90°. It appears that changes in this frequency of the plate are more affected by changes in the orientation of the SMA wires within the SMA/epoxy layers, than by changes in the orientation angle of the graphite fibers within the graphite/epoxy layers of the plate. The greatest performance of the plate is observed when the SMA wires are lengthwise orientated, which corresponds to the orientation angle of the SMA wires within the SMA/epoxy layers of 0°. For the cantilever plate boundary conditions the optimal orientation of the SMA wires within the SMA/epoxy layers for the greatest changes in the relative fundamental natural frequency of the plate is 0°, whereas the orientation of the graphite fibers within the graphite/epoxy layers is 45°. This corresponds to a ply stacking sequence of the plate of $[0°/(\pm45°)_5\ /0°]$. However, in the case of the simply-supported boundary condition the observed patterns are different as seen in

Figure 5. It is clear that the changes in the relative fundamental natural frequency of the plate are equally affected by both the changes in the orientation of the SMA wires within the SMA/epoxy layers, as well as by the changes in the orientation angle of the graphite fibers within the graphite/epoxy layers of the plate. For the simply-supported plate the optimal orientation of the SMA wires within the SMA/epoxy layers giving the greatest relative fundamental natural frequency of the plate is 45°, whereas the orientation of the graphite fibers within the graphite/epoxy layers are 0°/90° or 90°/0°. This corresponds to ply stacking sequences of the plate of [45°/(0°/90°)$_5$/ 45°].

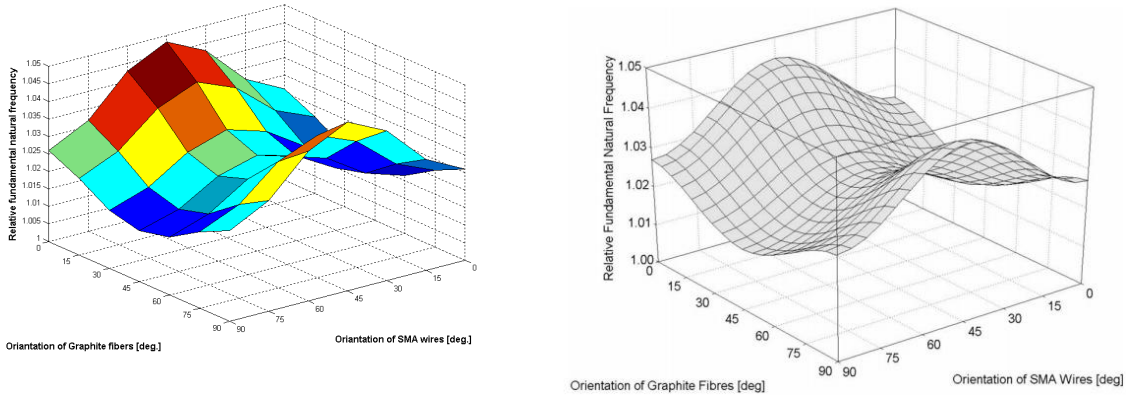

(a) Present model **(b) Zak [21]**

Figure 5. Change in the relative fundamental natural frequency of a simply-supported plate as a function of the orientation angle of graphite fibers and SMA wires.

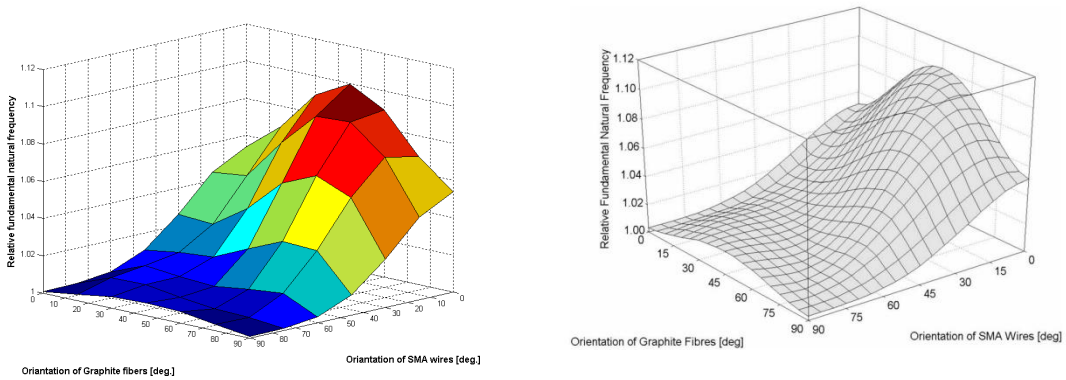

(a) Present model **(b) Zak [21]**

Figure 6. Change in the relative fundamental natural frequency of a cantilever plate as a function of the orientation angle of graphite fibers and SMA wires.

It is clear from Figure 5 and Figure 6 (a) and (b), that the obtained results are comparable with the published data obtained by Zak using the finite element technique with a mish size 8X8, [21].

The various mechanical properties of the composite material of the plate influence the plates relative fundamental natural frequency. The volume fraction of the SMA wires within the SMA/epoxy layers, as well as the volume fraction of the graphite fibers within the graphite/epoxy layers can also both vary. The influence of these changes on the relative frequency of the simply supported and the cantilever plate is investigated. It is shown in Figure 7 that the relative fundamental natural frequency of the plate increases with an increase in the volume fraction of the SMA wires, and with a decrease in the volume fraction of the graphite fibers. The maximum value of the relative fundamental natural frequency corresponds to the case when the outer layers of the plate are entirely made of the SMA material, whereas the inner layers are made of the epoxy resin. On the other hand when the volume fraction of the graphite fibers increases, the plate performance decreases rapidly, and

when the inner layers of the plate are entirely made of the graphite virtually no changes in the relative fundamental natural frequency of the plate are observed.

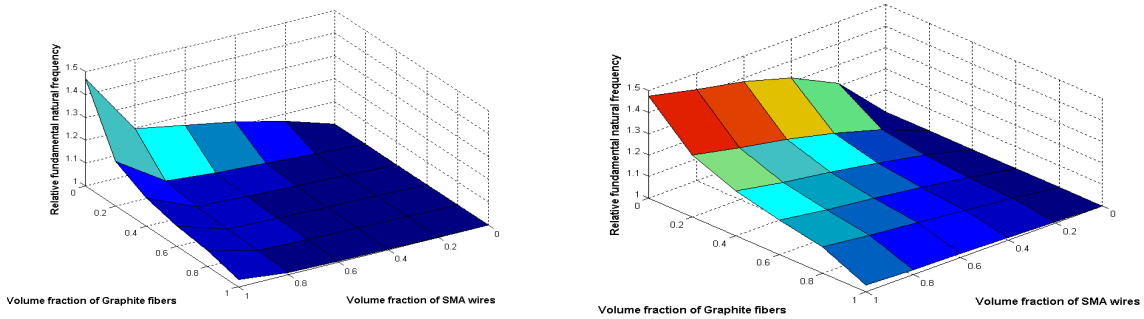

(a) Simply-supported plate (b) Cantilever plate

Figure 7. Change in the relative fundamental natural frequency as a function of the volume fraction of graphite fibers and SMA wires.

In Figure 8 the location of the SMA/epoxy layers z_s/h within the plate has a great influence on the plate performance. The location of the SMA/epoxy layers (z_s) within the plate can vary from the most extreme outer location to the central layers of the plate, and this corresponds to a ply stacking sequence change from $[0°/(\pm45°)_5/0°]$ to $[(\pm45°)_2/45°/(0°)_2/(-45°)/(\pm45°)_2]$. However, no assumptions are made regarding changes in the mechanical properties of the SMA/epoxy layers, or the graphite/ epoxy layers. From Figure 8, it arises that the relative fundamental natural frequency of the plate increases with a change in the location of the SMA/epoxy layer z_s/h. The changes in the relative fundamental natural frequency of the plate are much greater in the case of greater volume fractions of the SMA wires within the SMA/epoxy layers, and for the layers located closer to the extreme outer layers of the plate, than in the case of smaller volume fractions of the SMA wires within the SMA/epoxy layers, where the layers are located closer to the central layers of the plate. It is evident from the results presented in Fig. 8 that the plate performance is determined by the stiffness ratio of the SMA/epoxy layers and the graphite/epoxy layers. The stiffness of each material layer of the plate is also a function of the Young's modulus of the composite material components, as well as the position of the layer within the plate.

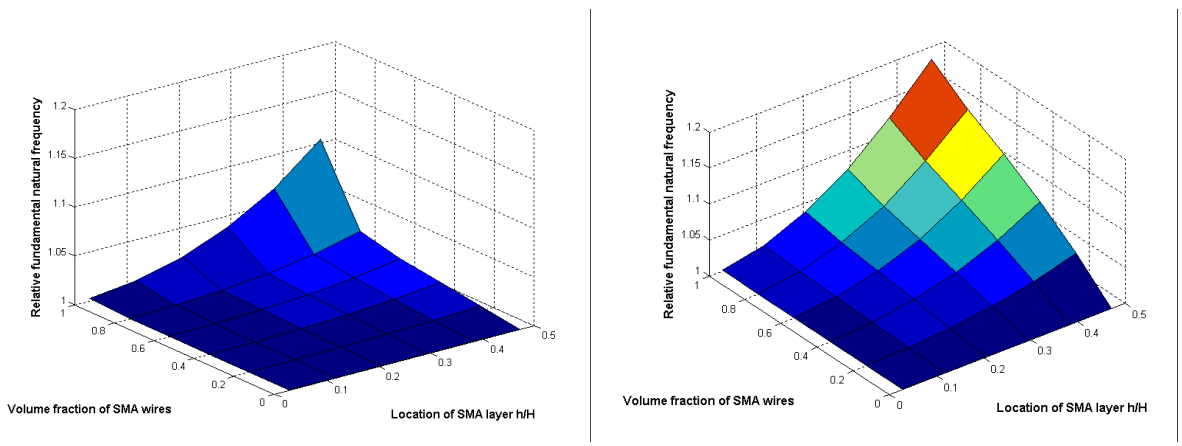

(a) Simply-supported plate (b) Cantilever plate

Figure 8. Change in the relative fundamental natural frequency as a function of the volume fraction of SMA wires and location of SMA wire layer.

10. Conclusion

An analytical model for laminated composite plates embedded with shape memory alloy wires was presented and analyzed based on the modified higher-order shear deformation theory using Ritz solution for simply-supported and cantilevered plates. The following conclusions have been drawn:

a) Both the plate dimensions and boundary conditions have a great influence on the relative fundamental natural frequency of the plate.

b) The relative fundamental natural frequency increases due to the activation of the SMA wires towards a longer and narrower plate of the cantilever boundary conditions. However, for simply-supported plate it increases toward a wider and shorter plate.

c) The relative fundamental natural frequency of the plate increases with an increase in the volume fraction of the SMA wires, and with a decrease in the volume fraction of the graphite fibers.

d) The maximum value of the relative fundamental natural frequency obtained when the outer layers of the plate are made by the SMA material, whereas the inner layers are made from the epoxy resin.

11. References

[1] M. M. Ghomshei, A. Khajepour, N. Tabandeh, and K. Behdinan "Finite element medeling of shape memory alloy composite actuators: theory and experiment" *Journal of intelligent material systems structures,* vol. 12, pp. 761-773, 2001.

[2] M. M. Ghomshei, N. Tabandeh, A. Khajepour, and K. Behdinan "Finite element analysis of a new shape memory alloy composite actuator" *http://resonance.uwaterloo.ca/students/mghomshei/ghomshe,* 2000.

[3] B. S. Balapgol, K. M. Bajoria, and Sudhakar "A two-dimensional finite element analysis of a shape memory alloy laminated composite plate" *Smart Materials and Structures, 15,* pp. 1009-1020, 2006.

[4] B. S. Balapgol, K. M. Bajoria, and Sudhakar "Natural frequencies of mutilayer SMA laminated composte cantilever plate" *Smart Materials and Structures, 15,* pp. 1021-1032, 2006.

[5] F. Gordaninejad and W. Wu "A two-dimensional shape memory alloy/elastomer actuator" *International Journal of Solids and Structures,* vol. 38, pp. 3393-3409, 2001.

[6] W. Wu, F. Gordaninejad, and R. A. Wirtz "Modeling and analysis of a shape memory alloy- elastomer composite actuator" *Journal of intelligent material systems structures,* vol. 7, pp. 441-447, 1996.

[7] C. A. Rogers, C. Liang and J. Jia "Structural modification of simply-supported laminated plates using embedded shape memory alloy fibers" *Computers & Structures,* vol. 38, pp. 569-580, 1991.

[8] M. W. Lin and C. A. Rogers "Analysis of stress distribution in a shape memory alloy composite beam" *Proceeding of the AIAA/ ASME/ AHS/ ASC 32nd structures, structural dynamics, and material conference , part 1,* vol. AIAA-91-1164-cp, pp. 169-177, 1991.

[9] K. Tanaka "A phenomenological description on thermomechanical behaviour of SMA," *Journal of Applied Mechanics,* vol. 112, pp. 158-163, 1990.

[10] C. Liang and C. A. Rogers "One-dimensional thermo-mechanical constitutive relations for shape memory materials" *Journal of intelligent material systems structures* vol. 1, pp. 207-234, 1990.

[11] L. C. Brinson and J. Mater "Constitutive behaviour of SMA: One-dimensional thermomechanical derivation with non-constant material functions and redefined martensite internal variable" pp. 729-743, 1990.

[12] L. C. Brinson "One-dimensional constitutive behavior of shape memory alloys: thermomechanical derivation with non-constant material functions and redefined martensite internal variable" *Journal of intelligent material systems structures*, vol. 4, pp. 229-242, 1993.
[13] A. Zak, M.P. Cartmell, W.M. Ostachowicz, and M.Wiercigroch " One dimensional shape memory alloy models for use with reinforced composite structures" *Smart Materials and Structures, 12,* pp. 338– 346, 2003.
[14] M. Achenbach and I. Muller "Simulation of material behaviour of alloys with shape memory" *Arch. Mech.*, vol. 37, No. 6, pp. 573-585, 1985.
[15] J. N. Reddy, *Mechanics of laminated composite plates and shells*, second ed.: CRC Press, 2004.
[16] Z. Guiping and T. Limin "A semi- analytical solution for thermal stress analysis of laminated composite plates in the Hamiltonian system" *Computers & Structures*, vol. 55, No. 1, pp. 113-118, 1995.
[17] R. M. Jones, *Mechanics of composite materials*, second ed.: Taylor & Francis, 1999.
[18] E. Livne and I. Navarro "Nonlinear equivalent plate modeling of wing-box structures" *Journal of Aircraft*, vol. 36, pp. 851-865, 1999.
[19] M. K. Abbas, M. Adnan Elshafei and Hany M. Negm "Modeling and Analysis of Laminated Composite Plate Using Modified Higher Order Shear Deformation Theory" in *15th International Conference on Aerospace Sciences & Aviation Technology, ASAT-15, May 28- 30*, MTC, Kobry Elkobbah, Cairo, Egypt, 2013, asat@mtc.edu.eg.
[20] M. K. Abbas "Design and Analysis of Aircraft Composite Structure Using Shape Memory Alloys" Master of Science, Chair of Aircraft Mechanical Engineering, Military Technical College, Cairo, 2013.
[21] A. J. Zak, M. P. Cartmell and W. M. Ostachowicz "A sinsitivity analysis of the dynamic performance of a composite plate with shape memory alloy wires" *Composite Structures*, vol. 60, pp. 145- 157, 2003.

Nomenclature:

α	Thermal expansion coefficient of the SMA material
$\{\gamma\}$	The unknown displacements vector
$\{\varepsilon\}$	Strain vector in x-y-z coordinates
$\{\sigma\}$	Stress vector in x-y-z coordinates
$[\bar{Q}]_i$	Transformed stiffness matrix of layer i
δU	Virtual strain energy
δV	Virtual work
δK	Virtual kinetic energy
$\{a(x,y)\}$	Column vectors of the Ritz approximation functions that satisfy the boundary conditions of the problem
$\{q(t)\}$	Column vectors of the Ritz coefficients
$[K]$	Stiffness matrix
$[M]$	Mass matrix
p_z, F_{zi}	Distributed and concentrated loads
$\{F\}$, $\{F_0\}$	Distributed and concentrated load vectors
A	Plate's area
a, b	Plate sides' dimensions

A, B, D	Extensional, coupling, and bending stiffness matrices
DOF	Degrees of freedom
E, F, H, J	Higher order stiffness matrices
h	Total laminate thickness
I_i	Inertia terms
k	Total number of layers
u	Displacement of a generic point in the plate in the x direction
u_0	Displacement of the geometric mid-plane in the x direction
v	Displacement of a generic point in the plate in the y direction
v_0	Displacement of the geometric mid-plane in the y direction
w	Displacement of a generic point in the plate in the z direction
w_0	Displacement of the geometric mid-plane in the z direction
θ_x	Rotation of the normal to the mid-plane about the y-axis
θ_y	Rotation of the normal to the mid-plane about the x-axis
θ_z	First order displacement factor
ξ_x, ξ_y	Third order displacements or warping functions
ψ_x, ψ_y, ψ_z	Second order displacements or warping functions

Appendix A.

The evolution equations that represent ξ_S and ξ_T as functions of stress and temperature:

1- Twinned Martensite $\rightarrow$ detwinned martensite

Or (Austenite $\rightarrow$ detwinned martensite)

a- $T > M_S$ and $\sigma_s^{cr} + C_M(T - M_S) < \sigma < \sigma_f^{cr} + C_M(T - M_S)$

$$\xi_S = \frac{1-\xi_{S0}}{2}\cos\left[\frac{\pi}{\sigma_s^{cr} - \sigma_f^{cr}}\left(\sigma - \sigma_f^{cr} - C_M\left(T - M_s\right)\right)\right] + \frac{1+\xi_{S0}}{2} \tag{A-1}$$

$$\xi_T = \xi_{T0} - \frac{\xi_{T0}}{1-\xi_{S0}}\left(\xi_S - \xi_{S0}\right) \tag{A-2}$$

b- $T < Ms$ and $\sigma_s^{cr} < \sigma < \sigma_f^{cr}$

$$\xi_S = \frac{1-\xi_{S0}}{2}\cos\left[\frac{\pi}{\sigma_s^{cr} - \sigma_f^{cr}}\left(\sigma - \sigma_f^{cr}\right)\right] + \frac{1+\xi_{S0}}{2} \tag{A-3}$$

$$\xi_T = \xi_{T0} - \frac{\xi_{T0}}{1-\xi_{S0}}\left(\xi_S - \xi_{S0}\right) + \Delta_{T\xi} \tag{A-4}$$

If $M_f < T < M_S$ and $T < T_0$

$$\Delta_{T\xi} = \frac{1-\xi_{T0}}{2}\left\{\cos\left[a_M\left(T - M_f\right)\right] + 1\right\}$$

else, $\Delta_{T\xi} = 0$ .g

2- Martensite $\rightarrow$ Austenite

For $T > A_S$ and $C_A(T - A_f) < \sigma < C_A(T - A_S)$

$$\xi = \frac{\xi_0}{2}\left\{\cos\left[\frac{\pi}{A_f - A_S}\left(T - A_S - \frac{\sigma}{C_A}\right)\right] + 1\right\} \qquad \text{(A-5)}$$

$$\xi_S = \xi_{S0} - \frac{\xi_{S0}}{\xi_0}(\xi_0 - \xi) \qquad \text{(A-6)}$$

$$\xi_T = \xi_{T0} - \frac{\xi_{T0}}{\xi_0}(\xi_0 - \xi) \qquad \text{(A-7)}$$

3- Austenite $\rightarrow$ Twinned Martensite

For $M_f < T < M_s$, $\sigma < \sigma_s^{cr}$ and $T < T_0$

Putting ξ_S and ξ_{S0} in Eq. (A-1) gives the same formula of Liang's model if we put the slope $C_M = \infty$ because the transformation curves at $\sigma < \sigma_s^{cr}$ are vertical lines as shown in Figure A1 [12],

$$\xi = \frac{1-\xi_0}{2}\cos\left[a_M\left(T - M_f\right)\right] + \frac{1+\xi_0}{2} \qquad \text{(A-8)}$$

In this case, the total induced martensite is a pure temperature induced martensite, i.e. $\xi = \xi_T$ and $\xi_0 = \xi_{T0}$.

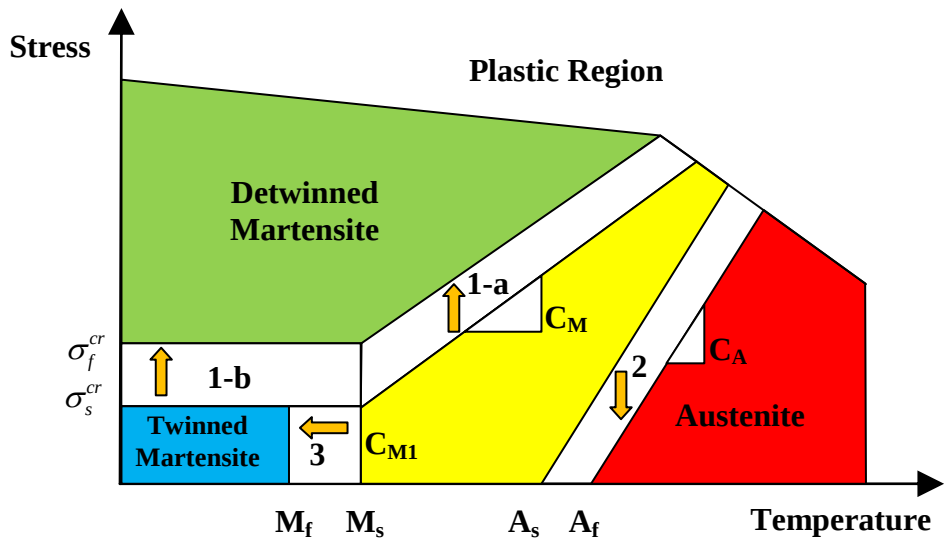

Figure A1. The effect of stress on the transformation temperature [12].

Appendix B.

The vector of thermal expansion coefficients $\{\alpha_i\}$ and the vector of SMA recovery stress $\{\sigma_i^r\}$ referred to the body (x-y-z) coordinate system.

$$\alpha_x = \alpha_{11}\cos^2\theta + \alpha_{22}\sin^2\theta, \alpha_y = \alpha_{11}\sin^2\theta + \alpha_{22}\cos^2\theta$$

$$\alpha_z = \alpha_3,\ \alpha_{yz} = 0,\ \alpha_{zx} = 0, \alpha_{xy} = (\alpha_{11} - \alpha_{22})\sin\theta\cos\theta$$

$$\sigma_x^r = \sigma_r\cos^2\theta, \sigma_y^r = \sigma_r\sin^2\theta$$

$$\sigma_z^r = 0,\ \sigma_{yz}^r = 0,\ \sigma_{zx}^r = 0, \sigma_{xy}^r = \sigma_r\sin\theta\cos\theta$$

Appendix C. The used column vectors of the Ritz approximation functions for simply supported boundary conditions are:

$$\{a_1(x,y)\}^T=\left[\left(y^2-by\right)\left(2x-a\right)\right],\{a_2(x,y)\}^T=\left[\left(x^2-ax\right)\left(2y-b\right)\right]$$

$$\{a_3(x,y)\}^T=\left[\bar{X}\bar{Y}\quad \bar{X}^2\bar{Y}\quad \bar{X}\bar{Y}^2\quad \bar{X}^2\bar{Y}^2\quad \bar{X}^3\bar{Y}\quad \bar{X}\bar{Y}^3\right],$$

$$\{a_4(x,y)\}^T=\left[\left(1-\frac{6x^2}{a^2}+\frac{4x^3}{a^3}\right)\left(y-\frac{2y^3}{b^2}+\frac{y^4}{b^3}\right)\right],\{a_5(x,y)\}^T=\left[\left(x-\frac{2x^3}{a^2}+\frac{x^4}{a^3}\right)\left(1-\frac{6y^2}{b^2}+\frac{4y^3}{b^3}\right)\right]$$

$$\{a_6(x,y)\}^T=\left[1\quad \left(x-\frac{2x^3}{a^2}+\frac{x^4}{a^3}\right)\left(y-\frac{2y^3}{b^2}+\frac{y^4}{b^3}\right)\right],\{a_7(x,y)\}^T=\left[\left(y^2-by\right)\left(2x-a\right)\right]$$

$$\{a_8(x,y)\}^T=\left[\left(x^2-ax\right)\left(2y-b\right)\right],\{a_9(x,y)\}^T=\left[1\quad \left(x-\frac{2x^3}{a^2}+\frac{x^4}{a^3}\right)\left(y-\frac{2y^3}{b^2}+\frac{y^4}{b^3}\right)\right]$$

$$\{a_{10}(x,y)\}^T=\left[\left(1-\frac{6x^2}{a^2}+\frac{4x^3}{a^3}\right)\left(y-\frac{2y^3}{b^2}+\frac{y^4}{b^3}\right)\right],\{a_{11}(x,y)\}^T=\left[\left(x-\frac{2x^3}{a^2}+\frac{x^4}{a^3}\right)\left(1-\frac{6y^2}{b^2}+\frac{4y^3}{b^3}\right)\right]$$

Appendix D. The used column vectors of the Ritz approximation functions for a cantilever plate are:

$$\{a_1(x,y)\}^T=\left[x\quad xy\quad x^2\quad x^2y\right]_{1x\,4}$$

$$\{a_2(x,y)\}^T=\left[x^2\quad x^2y\quad x^3\quad x^3y\right]_{1x\,4}$$

$$\{a_3(x,y)\}^T=\left[x^2\quad x^2y\quad x^3\quad x^2y^2\quad x^3y\quad x^4\quad x^3y^2\quad x^4y\quad x^4y^2\right]_{1x\,9}$$

$$\{a_4(x,y)\}^T=\left[x\quad xy\quad x^2\quad x^2y\right]_{1x\,4},\{a_5(x,y)\}^T=\left[x\quad xy\quad x^2\quad x^2y\right]_{1x\,4}$$

$$\{a_6(x,y)\}^T=\left[1\quad x\quad y\quad xy\right]_{1x\,4},\{a_7(x,y)\}^T=\left[x\quad xy\quad x^2\quad x^2y\right]_{1x\,4}$$

$$\{a_8(x,y)\}^T=\left[x\quad xy\quad x^2\quad x^2y\right]_{1x\,4},\{a_9(x,y)\}^T=\left[1\quad x\quad y\quad xy\right]_{1x\,4}$$

$$\{a_{10}(x,y)\}^T=\left[x\quad xy\quad x^2\quad x^2y\right]_{1x\,4},\{a_{11}(x,y)\}^T=\left[x\quad xy\quad x^2\quad x^2y\right]_{1x\,4}$$